









Finite-size correlation behavior near a critical point: A simple metric for monitoring the state of a neural network

Eyisto J. Aguilar Trejo ^{1,2} Daniel A. Martin ^{1,2,*} Dulara De Zoysa ³ Zac Bowen ⁴ Tomas S. Grigera ^{2,5,6,7}
Sergio A. Cannas ^{2,8} Wolfgang Losert ³ and Dante R. Chialvo ^{1,2}

¹*Instituto de Ciencias Físicas (ICIFI-CONICET), Center for Complex Systems and Brain Sciences (CEMSC3), Escuela de Ciencia y Tecnología, Universidad Nacional de Gral. San Martín, Campus Miguelete, 25 de Mayo y Francia, 1650, San Martín, Buenos Aires, Argentina*

²*Consejo Nacional de Investigaciones Científicas y Técnicas (CONICET), Godoy Cruz 2290, 1425, Buenos Aires, Argentina*

³*Department of Physics & Institute for Physical Science and Technology, University of Maryland, College Park, Maryland 20742, USA*

⁴*Fraunhofer USA Center Mid-Atlantic, Riverdale, Maryland 20737, USA*

⁵*Departamento de Física, Facultad de Ciencias Exactas, Universidad Nacional de La Plata, 1900, La Plata, Buenos Aires, Argentina*

⁶*Instituto de Física de Líquidos y Sistemas Biológicos (IFLySiB-CONICET) Universidad Nacional de La Plata, 1900, La Plata, Buenos Aires, Argentina*

⁷*Istituto dei Sistemi Complessi, Consiglio Nazionale delle Ricerche, via dei Taurini 19, 00185 Rome, Italy*

⁸*Instituto de Física Enrique Gaviola (IFEG-CONICET), Facultad de Matemática Astronomía Física y Computación, Universidad Nacional de Córdoba, 5000, Córdoba, Argentina*



(Received 20 August 2022; accepted 28 October 2022; published 29 November 2022)

In this article, a correlation metric κ_c is proposed for the inference of the dynamical state of neuronal networks. κ_c is computed from the scaling of the correlation length with the size of the observation region, which shows qualitatively different behavior near and away from the critical point of a continuous phase transition. The implementation is first studied on a neuronal network model, where the results of this new metric coincide with those obtained from neuronal avalanche analysis, thus well characterizing the critical state of the network. The approach is further tested with brain optogenetic recordings in behaving mice from a publicly available database. Potential applications and limitations for its use with currently available optical imaging techniques are discussed.

DOI: [10.1103/PhysRevE.106.054313](https://doi.org/10.1103/PhysRevE.106.054313)

I. INTRODUCTION

The study of critical phenomena in the brain [1–3] benefited from different experimental approaches. The most common by far is the statistical characterization of the so-called neuronal avalanches, consisting of sudden increases in the activity which exhibits power-law distribution of sizes and durations [4]. This analysis has been reproduced over different setups (i.e., tissues and experimental conditions, see, e.g., Refs. [5,6]), and in a diversity of numerical simulations. The resulting statistics represent a long-term average estimation over thousands of avalanches, spanning very long periods of time, making the approach unsuitable for tracking fast dynamical changes. Several caveats, such as subsampling [7], thresholding [8], or the artifacts introduced by the coexistence of overlapping avalanches [9], as well as alternative interpretations of the results [10] prompted the exploration of complementary approaches.

One of them, which is very often documented on continuous phase transitions, is the behavior of the correlation length ξ , which diverges with the size of the system at the critical point (see, e.g., Ref. [11]), a fact that was shown to be exhibited by the large-scale brain dynamics [12,13].

More recently the same divergence of ξ was demonstrated in the behaving mice brain [14,15]. These measures were facilitated by the use of novel optogenetic techniques [16], which allows for the recording of the individual activity of a relatively large number of neurons. In that work, a proxy of the standard finite-size analysis, named box-scaling, was used, [17] in which the observation window, instead of the system size, is varied. An estimate of the correlation length ξ was found to grow linearly or logarithmically with window size depending if the system is near or far from the critical state, respectively. Based on these previous results, the purpose of this Letter is to introduce a simple metric, describing the typical finite-size behavior of the correlation length near criticality to distinguish critical from noncritical dynamics. To this end, we study a simple model of neuronal dynamics that can be tuned toward and away from the critical point of a second-order phase transition dynamics as the control parameter is varied. We contrast the new metric with the most common analysis, the avalanche size distribution statistics.

The paper is organized as follows: In Sec. II, we describe the model and define the observables, first for the standard metric of avalanches analysis and then for the finite-size correlation based metric. In Sec. III, the main results are described by contrasting the metrics in both numerical and experimental data. The paper closes with a short discussion of the limitations and potential applications in Sec. IV.

*dmartin@unsam.edu.ar

II. MODEL AND OBSERVABLES

The model, previously described [13,17,18], is a cellular automata based on the Greenberg and Hastings model [19], running on a two-dimensional lattice of $L \times L$ neurons under periodic boundary conditions. Each neuron j has $k = 24$ output connections chosen as follows: the closest k neurons are initially connected, and then, to mimic a small world topology, each of these connections is rewired with probability $\pi = 0.01$ to another, randomly chosen, postsynaptic neuron within the whole system. The resulting k nonzero connection weights are taken randomly from an exponential distribution $p(W_{ij} = w) \propto \exp(-w\lambda)$ with $\lambda = 12.5$ (as in Ref. [18]). The connection matrix is fixed and does not need to be symmetric. Time is considered discrete and each neuron i may be in any of the following three states: quiescent [$S_i(t) = 0$], active [$S_i(t) = 1$], or refractory [$S_i(t) = 2$]. At time $t + 1$ a quiescent neuron can become active due to an external input with a small probability r_1 (we have used $r_1 = 10^{-5}$), or if the contribution of all active connections at time t is larger than a threshold T ($\sum_j W_{ij} \delta_{S_j(t),1} > T$); an active neuron will become refractory always, and a refractory neuron will become quiescent with probability r_2 (following Ref. [18], we have used $r_2 = 0.3$ throughout the text). The computer codes for numerical simulations and data analyses can be found in Ref. [20]. An important remark is that the results rely on universal behavior of the correlation function in critical phenomena, thus they are model independent.

We run simulations for several values of the control parameter T which previous results [17] indicate produces subcritical (for very high values of T), supercritical (for very low values of T), or critical dynamics. To accumulate enough statistics, we run 20 numerical simulations (lasting 10^5 time steps, discarding the initial 5000 time steps). For each simulation we constructed a different network with the same parameters k and π (i.e., the networks are stochastic realizations each with different randomly chosen rewired connections and connection weights). To mimic experimentally relevant situations, we record the dynamics of the neurons within a square window size of $W \times W$ neurons (with $W \leq L$), see Fig. 1(a).

A. Metric based on avalanche size distribution

The standard procedure for avalanche analysis [4] focuses on the estimation of the distribution of avalanche size and duration. For that, the total activity of the neurons inside a given (spatial) window is computed as a function of time, $A(t) = \sum_{i \in W \times W} \delta_{S_i(t),1}$ [$S_i(t) = 1$ if neuron i is spiking at time t]. Notice that, in the standard procedure, it is usual to group the activity on time bins approximately equal to the average of all interspike intervals. The coarse grain scale of the model considered here (i.e., only three discrete states) determines that we must compute $A(t)$ for each time unit, as mentioned above. Also, since for the conditions in our case $A(t)$ very rarely becomes zero, following Ref. [8], we need to define a nonzero avalanche threshold c . Avalanche size s is defined then as the total activity above c between two consecutive zeros of $A(t) - c$ [i.e., $s = \sum_i [A(t) - c]$, where the sum is performed over the avalanche duration], see Fig. 1(b). At criticality, avalanche

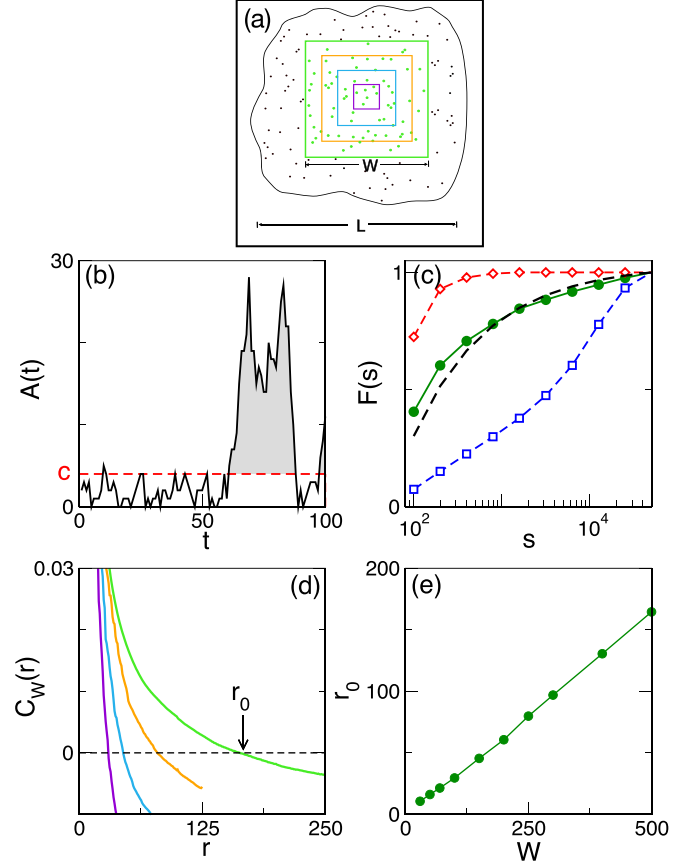


FIG. 1. System scheme. (a) A system of characteristic size L is studied through boxes of side W . Only neurons inside the box are recorded. (b) Example of the time series of A , the total number of active neurons inside a window, as a function of time. An avalanche (filled with gray) is defined as the total activity above a threshold c , computed from the time at which A becomes greater than c to the next time that it becomes lower than c . Panel (c) shows the cumulative avalanche size distribution function $F(s)$ as a function of avalanche size s for three different situations: subcritical ($T = 0.33$, open blue squares), supercritical ($T = 0.31$, open red diamonds), and close to criticality ($T = 0.318$ green filled circles). The dashed line represents the theoretical expectation for the avalanche size distribution expected at criticality, $F^{NA}(s)$. Curves were computed for $m = 10$ values of s . (d) The connected correlation function of a window of size W , $C_W(r)$, for several values of W , computed at criticality. From left to right, $W = 50$ (violet line), $W = 150$ (cyan), $W = 250$ (orange), $W = 500$ (light green). The characteristic length r_0 for $W = 500$ is marked with an arrow, as an example. (e) Characteristic length r_0 as a function of window size W at the critical state. Results computed on a system of size $L = 1000$, $k = 24$, $\pi = 0.01$, and $T = 0.318$. In panels (b) and (c), a window size $W = 500$ was used.

size distribution $P(s)$ is expected to have a power-law distribution, $P(s) \propto s^{-\tau}$, where, in the mean field directed percolation universality class, $\tau = 3/2$ [4,21]. The value of c is chosen to maximize the number of avalanches for each value of T and W .

The goodness of fit of the neuronal avalanches size distribution to a power law has been considered as suggestive for critical dynamics, which taken in isolation may call for

caveats, precautions, and criticisms [22]. Nonetheless, when used in conjunction with other measures it can overcome some of its limitations [10]. In that regard, Shew *et al.* [23] defined, from the observed cumulative avalanche size distribution $F(s)$, a metric κ_S , which is [23]

$$\kappa_S = 1 + \frac{1}{m} \sum_{k=1}^m F^{NA}(\beta_k) - F(\beta_k), \quad (1)$$

where $F^{NA}(\beta) = [1 - (s_{\min}/\beta)^{\tau-1}]/[1 - (s_{\min}/s_{\max})^{\tau-1}]$ is the theoretical distribution for the critical case, and β_k are m logarithmically spaced values ranging from $s_{\min} = 50$ to $s_{\max} = 50000$. We have used $m = 10$ as in Ref. [23]. An example of $F(s)$ and F^{NA} is shown in Fig. 1(c). For power-law avalanche size distributions with exponent $\tau = 3/2$, the cumulative avalanche size distribution $F(s)$ will be equal to $F^{NA}(s)$, then a value of $\kappa_S = 1$ is expected, while $\kappa_S \geq 1$ for super or subcritical conditions.

B. Metric based on finite-size scaling of correlations

Following previous work [17], we computed the connected correlation function on a window of size W , as the correlation of the fluctuations of the neuronal activity, with respect to its *instantaneous spatial average* [12–14,17,24–30]:

$$C_W(r) = \frac{1}{c_0} \frac{\sum_{i,j} \delta v_i \delta v_j \delta(r - r_{ij})}{\sum_{i,j} \delta(r - r_{ij})}, \quad (2)$$

where $\delta(r - r_{ij})$ is a smoothed Dirac δ function selecting pairs of neuron states at a distance r [in practice, we have computed $C_W(r)$ for integer values of r , averaging all points at distances $(r - 0.5, r + 0.5)$]; r_{ij} is the Euclidean distance from the site i to site j ; δv_i is the value of the signal v_i of site i at time t , after subtracting the *instantaneous spatial average* of signals $V(t) = (1/N) \sum_i v_i(t)$, i.e., $\delta v_i(t) = v_i(t) - V(t)$; and $1/c_0$ is a normalization factor to ensure that $C_W(r = 0) = 1$. We consider that $v_i = 1$ if neuron i is in the active ($S_i = 1$) or refractory ($S_i = 2$) state and $v_i = 0$ otherwise. Although $C_W(r)$ can be computed on a single snapshot [in contrast with $F(s)$], to improve statistics, we average the result over several time steps. We compute Eq. (2) once every 20 time steps (i.e., we take information for 4750 [31] time steps for each network), and then average the result over different time steps and different networks. An estimate of the correlation length can be calculated from Eq. (2) as r_0 , the first zero crossing of the function [i.e., $C_W(r_0) = 0$]. An example of $C_W(r)$, for different values of W is shown in Fig. 1(d), while r_0 as a function of W , is shown in Fig. 1(e). We remark that the implementation of r_0 estimates correlations computed inside a window, after subtracting the *instantaneous* spatial average. This differs from the frequently considered connected correlation function, computed from the fluctuations of each variable with respect to their time average (although, for systems in equilibrium thermodynamics, they are equivalent [28]). This characteristic makes $C_W(r)$ in Eq. (2), immune to global trends and hidden confounders, as discussed elsewhere [17,29].

We measure $C_W(r)$ for several values of W ranging from W_{\min} to W_{\max} . For equilibrium thermodynamic systems, the behavior of r_0 as a function of W , for fixed L , is known

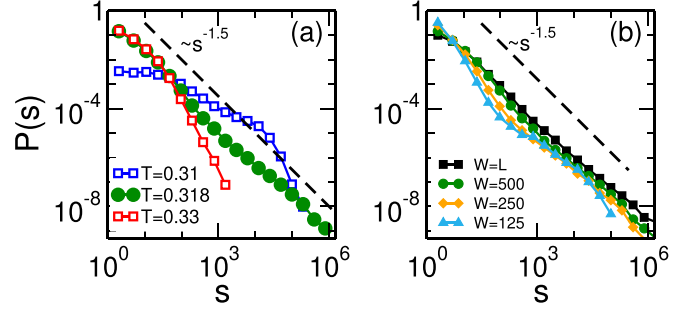


FIG. 2. Avalanche size distribution computed on a window of size $W = 500$, for different values of T in panel (a) and for $T = 0.3180 \simeq T_C$ and several values of W in panel (b). The dashed lines, in both panels, show a power law with exponent $-3/2$ as a guide to the eye. All parameters are the same as in Fig. 1.

in the limiting cases: $r_0 \propto W$ for $W \ll L \ll \xi$ at criticality, while $r_0 \propto \xi \ln(W/\xi)$ for $\xi \ll W_{\min}$, where ξ is the standard correlation length, see Refs. [17,28].

To estimate the distance to criticality, for each explored window size W_i , we propose a linear relation between $r_0(W_i)$ and W_i : $r_0(W_i) = a_i \times W_i$, and extract the value of the slope a_i from the data [32]. Also, we propose a logarithmic growth $r_0(W_i) = r_0(W_{\min}) + b_i \ln(W/W_{\min})$. Similar to Eq. (1), we define

$$\kappa_C = \frac{CV_s^2}{CV_c^2 + CV_s^2}, \quad (3)$$

where CV_s is the coefficient of variation of $\{b_i\}$, and CV_c is the coefficient of variation of $\{a_i\}$, see Ref. [20]. Notice that $0 \leq \kappa_C \leq 1$, where $\kappa_C = 0$ is for a perfect logarithmic growth and $\kappa_C = 1$ is for perfect linear growth. While more sophisticated measures can be proposed, the definition of (3) is simple and insensitive to changes in the spatial scale ($r \rightarrow \lambda r$).

III. RESULTS

As a reference, we first characterize the behavior of the avalanche size distribution, computed inside of a window of size $W = 500$, for different values of T . The results are shown in Fig. 2(a). In the subcritical state ($T = 0.33$), activity is low, and there are no large avalanches, for any value of c . In the supercritical case ($T = 0.31$), activity is very high, being always larger than zero. The avalanche size distribution has a hump for $s \approx 10^5$. Hump position depends on c , showing system-wide avalanches (commonly dubbed “dragon kings”) for low values of c . In the critical case ($T \simeq 0.318$), avalanche size distribution follows closely a power law with exponent $\tau = 3/2$. Different values of τ , in the range [1.3–1.7], can be estimated for different values of c . For the critical data in the figure [line with circles in Fig. 2(a)], it can be seen that, for small values of s (i.e., $s < 100$), there is an excess of avalanches compared with the expected. This excess is a consequence of subsampling and is not present for $W = L$, while it is even larger for small values of W , such as $W = 125$, see Fig. 2(b). This difference may be due to the contributions of avalanches that enter or leave the window from the rest of the system, as already discussed in the context

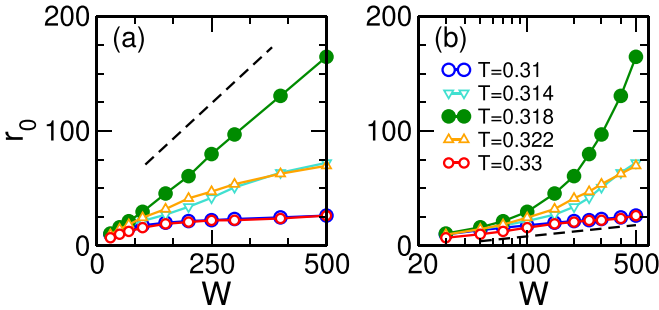


FIG. 3. Characteristic correlation length as a function of window size W obtained at various control parameter values T (indicated in the legend). The same results are plotted on a linear scale in panel (a) and on a linear-logarithmic scale in panel (b). All other parameters are the same as in Fig. 1.

of avalanches in the quenched Kardar-Parisi-Zhang (qKPZ) model, see Ref. [33].

Next, we turn to describe the correlation behavior on the same data used to study avalanches. The characteristic correlation length r_0 as a function of window size W , for $W_{\min} = 30$, $W_{\max} = 500$, is shown in Fig. 3. For the critical value of the threshold ($T = 0.318$), there is a linear relation between r_0 and W , while for sub and supercritical regimes, r_0 is smaller, and the growth of r_0 with W is logarithmic. Slightly subcritical and supercritical cases (plotted with triangles), show intermediate results. Similar results can be found when $C_W(r)$, Eq. (2), is computed for the whole system ($W = L$), varying system size, as shown in Ref. [17] for the Ising paramagnetic-ferromagnetic model and for a different neuronal model [7].

The values of κ_S and κ_C , extracted from avalanche size distribution and correlation length scaling, are shown in Fig. 4. Avalanche analysis (κ_S), assuming $\tau = 3/2$, yields expected results: $\kappa_S > 1$ (< 1) for the supercritical (subcritical) regime, while κ_S is closest to 1 for the critical regime, $T = 0.318$ (marked with a green dot). For very subcritical values (high T), κ_S does not keep on decreasing, probably due to having a short range of s values captured by $P(s)$. The analysis of characteristic length collapse, κ_C , shows compatible results, see Fig. 4(b). The linear fit is better than the logarithmic fit (i.e., $\kappa_C > 0.5$) only for $0.314 < T < 0.322$, having its peak at $T = 0.318$, i.e., the same value as in κ_S .

For completeness, in Fig. 4(c) we also show the first autocorrelation coefficient of the activity, $AC(1)$ which by

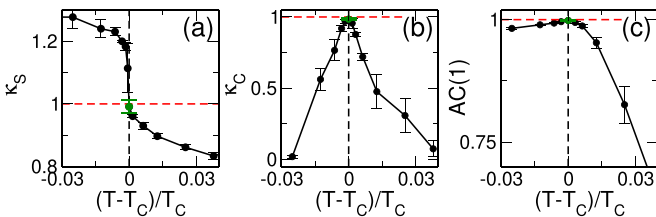


FIG. 4. Behavior of the different metrics (mean \pm SD) as a function of T near the critical point of the neural model: κ_S in panel (a) and κ_C in panel (b) and $AC(1)$ in panel (c). All other parameters are the same as in Figs. 2 and 3.

definition is always smaller than 1, and reaches a maximum at criticality [34]. $AC(\Delta t)$ is computed from the activity $A(t)$ on the largest window ($W = 500$) as $AC(\Delta t) = \langle A(t + \Delta t) - \langle A \rangle \rangle \times \langle A(t) - \langle A \rangle \rangle / [\langle A(t)^2 \rangle - \langle A(t) \rangle^2]$, where $\langle \dots \rangle$ stands for temporal average. The critical value of T derived from $AC(1) = AC(\Delta t = 1)$ also coincides with results from κ_C and κ_S .

To compare the performance of κ_S , κ_C , and $AC(1)$, in Fig. 5, we show the metric's behavior as a function of slow variations of the control parameter T . In Fig. 5(b), we show how the control parameter T is varied as a function of time, generating a nonstationary activity time series [see the raster plot for a few neurons in Fig. 5(a)]. The values of κ_S , κ_C , and $AC(1)$, computed on time segments of $n = 2000$ steps, are shown in Figs. 5(c) and 5(d). It can be seen that, close to criticality (i.e., $T = T_C$), the variability in κ_C is lower than the variability in κ_S . We also show the first autocorrelation coefficient of the activity, $AC(1)$ [see Fig. 5(d)], which shows a low variability in the critical (and supercritical) regime.

To study this observation in depth, we run four independent simulations on the same network (with different annealed noise), at fixed $T = T_C$, for 40 000 steps each. Using all these data (i.e., all the time frames from all the runs), we compute the expected values κ_S^* , κ_C^* , and $AC(1)^*$. Next, we compute κ_S , κ_C , and $AC(1)$ using several short segments of the time series, of length n (from $n = 400$ to $n = 40\,000$). We define the *Error* as the average distance (computed as the absolute difference) of these values to the expected values κ_S^* , κ_C^* , and $AC(1)^*$. For all observables, the *Error* decays with the number n of samples used [see Fig. 5(e)]. For samples with $n > 1000$, we find that the *Error* in κ_C [and $AC(1)$] is lower than the *Error* in κ_S . More important, the error of κ_C and $AC(1)$ decay as $\approx 1/n$, faster than for κ_S .

Novel optogenetic imaging techniques allow for the simultaneous recordings of the activity of hundreds of neurons [16], an optimal setting to compare the statistical measures. Figures 6 and 7 show the behavior of the proposed metrics to characterize the dynamics of a selected dataset from the Allen Institute's Brain Observatory [35], recorded (at 30 Hz for 114 099 time frames) from a conscious mouse. The data corresponds to the inferred spike probabilities of 295 neurons inside a field of view of $400 \times 400 \mu\text{m}$ in the VISp area. These data set were selected because its experimental design includes the presentation of different visual stimuli. We expected that the stimuli shall induce variations on the neuronal network state large enough to be reflected consistently on the metrics described here. Previous analyses on rat visual cortexes [36], subject to monocular deprivation, and turtles subject to visual stimulation [37] showed that the stimulation changes the dynamical state in ways that were measurable by using computations related to avalanche size distribution and other proposed observables.

First we explored the behavior of the metrics as a function of the number of samples (i.e., frames). Figure 6 a shows the box-scaling results, calculated from the spike time series extracted from [35]. A linear relation between W and r_0 is observed for all $W \gtrsim 100 \mu\text{m}$, while this relation breaks at shorter distances. From this observation, we estimate a characteristic interaction length of the order of $100 \mu\text{m}$, which

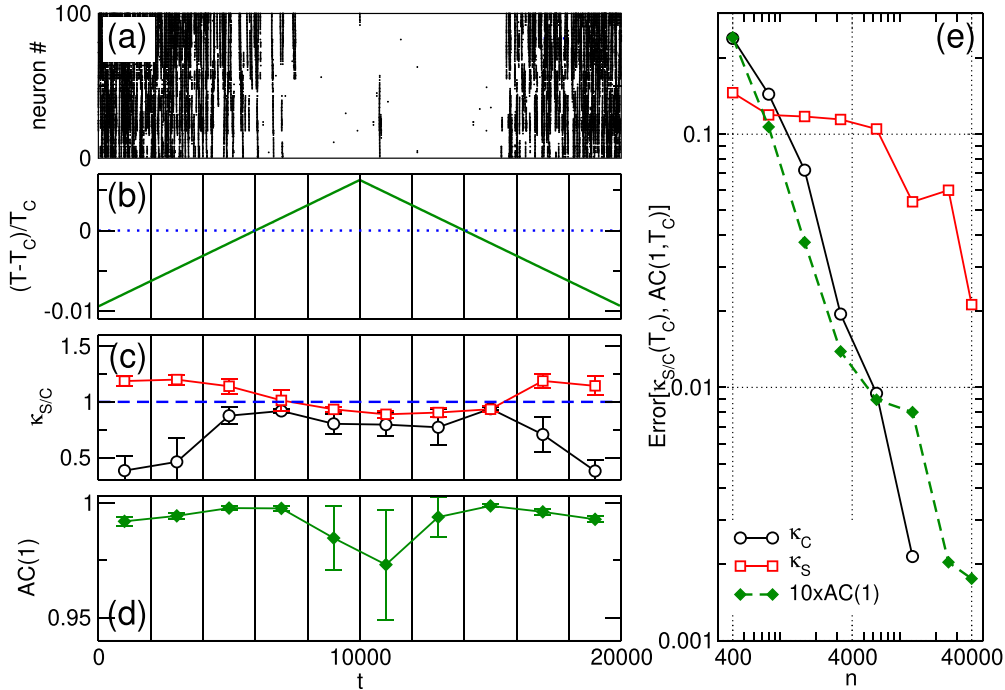


FIG. 5. Numerical simulations demonstrating the behavior of the metrics in response to a slow change in the network excitability, here simulated by ramping up and down the model parameter T . Panel (a) shows the raster plot of a subset of 100 neurons as T is varied. Panel (b) shows the evolution of T as a function of time t . Panel (c) shows the estimated mean (\pm SD) κ_S and κ_C , computed over time segments of $n = 2000$ steps. For κ_C , we used spatial windows $W \leq 300$. For κ_S an average of ≈ 95 avalanches (range 14–280) were detected in each run and each temporal window. Panel (d) shows the first autocorrelation coefficient $AC(1)$ of the population rate fluctuations within the same windows. Panel (e) shows the errors of the estimators, computed as the average distance between the measured and the expected value, κ_S^* , κ_C^* , and $AC(1)^*$, as a function of the number n of steps at $T = 0.3180 \approx T_c$. Results in each panel are from four independent realizations of the numerical simulations. For avalanche analysis, since n is variable, we considered s_{\min} as 10 times the smaller avalanche size observed, and s_{\max} as 0.1 of the largest observed avalanche size.

is slightly shorter than (but comparable to) the experimental neuronal connection lengths [38]. The same data are plotted on a log-linear axis in the inset of that figure to emphasize its nonlogarithmic scaling (compare with results in Fig. 3). Figure 6(c) shows the avalanche size distribution computed from the same spike time series. The results approximate the expected power-law distribution for about two decades. The values of κ_C and κ_S , for different sampling length, are shown in Figs. 6(b) and 6(d). Note that, as expected, the range of κ_C and κ_S observed values broaden for shorter time series.

Next, we explored up to which degree the fluctuations, spontaneous or introduced by the visual stimuli, may be reflected on the proposed metrics. Figure 7 shows the results of analyzing the temporal fluctuations of the metrics computed in eight nonoverlapping temporal segments, each one corresponding to different visual stimuli. According to the analysis, throughout the segments the dynamics remain slightly subcritical, with variations depending on the type of stimulus. In consequence, the relative fluctuations of each metric are directly proportional to each other, as shown in Figs. 7(f)–(h). Note that the population rate [i.e., Fig. 7(b)], in this context, shall be considered as a pseudo-order parameter [34].

While inferring the dynamical state of the network is relevant on its own, another important question, in the context of brain dynamics, is how the dynamical state may affect the system's response. To address this question, we study how the

neurons' response depends on the network state. We define the response to a given stimulus as the firing rate change when the stimulus is turned on, compared with the rate immediately before, divided by the summed rate: $\text{Response} = (R_s - R_b)/(R_s + R_b)$, where R_s is the rate when the stimulus is present, averaged over all considered neurons and stimulus presentations, and R_b is computed over the same neurons, for time windows of the same duration, immediately before the stimulus onset. For static gratings, we say that a neuron responds to a given angle if the response is larger for that orientation than for gratings in any other direction. Similarly, we say that a neuron responds to a given natural image if the rate increase is larger for that image than for any other natural image.

Figure 8 shows the change in network responses for different network states, evaluated with different metrics. The results show that the *response* for static gratings is mostly insensitive to the changes in the dynamical state, while the response for natural images became larger when the state approaches criticality. We have limited the analysis to the eight natural images that generate the largest responses. The analysis is a pilot demonstration of two aspects that deserve to be better explored: on one side it shows the well-known fact that the response of the visual cortex is stronger for natural images, and on the other side, that when the metric indicates that the network is closer to criticality it maximizes its responses [23].

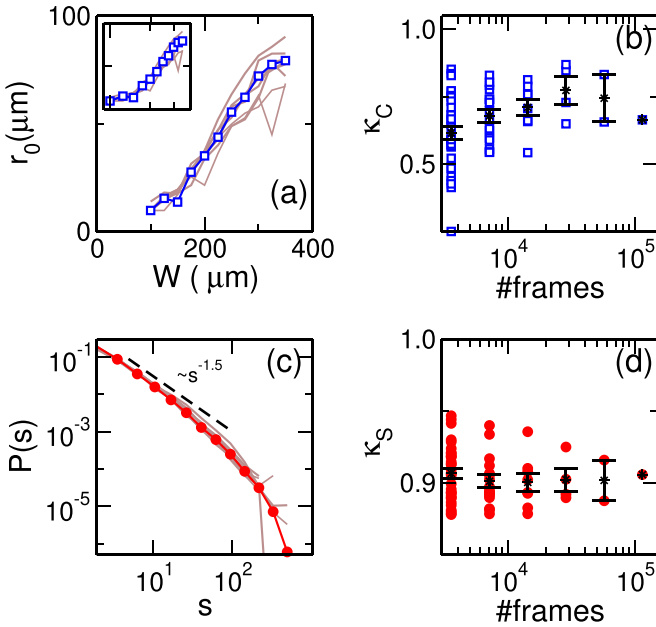


FIG. 6. Experimental recordings. Analysis of neuronal spike data inferred from two-photon imaging from the Allen Institute database [35]. Panel (a) shows box-scaling results for the entire data with empty symbols and with lines for the segments of 1/8 of the time series. The inset shows the same data in log-linear axis. In panel (b) the symbols show κ_C for different time windows as a function of the number of frames used, while the black lines show the mean \pm standard error. Panel (c) shows the avalanche size distribution of the same data, for all time frames with filled symbols (17 155 avalanches), and for segments of 1/8 of the points [as in panel (a)] with lines. Panel (d) shows the κ_S in the same format used in panel (b). For each time segment, κ_C was computed from windows of size 100 μm or larger, while κ_S was computed using avalanche sizes ranging from twice the minimum observed avalanche size to half of the largest observed avalanche size.

IV. DISCUSSION

It is known that the status of cortical networks changes following spontaneous fluctuations in excitability, arousal, sleep, vigilance or in response to sensory inputs or anesthetic agents. A simple approach to track these changes is the computation of the pair-wise mutual correlations, which at the critical state exhibits scale invariance. A motivation for the present work is to develop practical methods for tracking these changes in the global correlations of a network, under the assumption that such quantification may help to understand cortical responses under a variety of changing circumstances.

New methods shall take advantage of the novel optogenetic techniques which not only provide data from a very large number (hundreds to thousands) of neurons but also provide spatial information. In contrast, the avalanche analysis only relies on counting the number of neurons firing at any given time, not profiting from the abundance of spatial information offered by optogenetic techniques. The metric proposed here, based on the computation of the connected correlation length, is performed from instantaneous snapshots of the system. By construction, this feature gives the approach some important

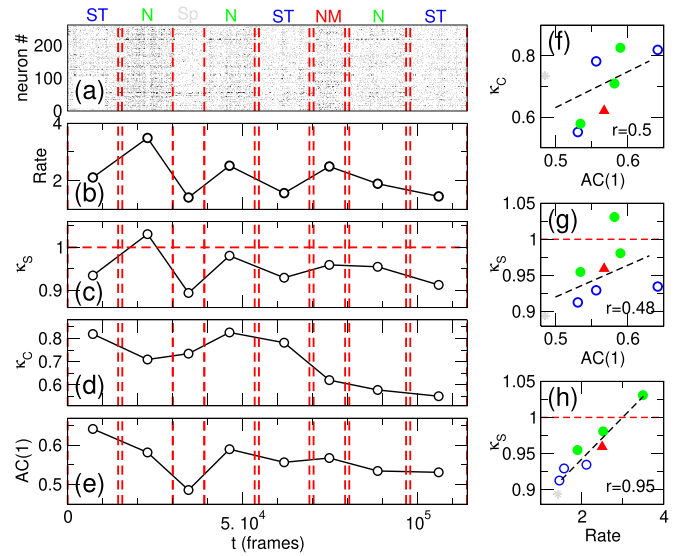


FIG. 7. Dynamical changes in response to visual stimuli exhibited by the experimental recordings according with the different metrics (same data as in Fig. 6). Panel (a) shows the raster plot, and panel (b) shows the average rate (number of spikes per frame) computed over time blocks related to different visual stimuli. Panels (c) through (e) show κ_S , κ_C , and $AC(1)$, respectively, for the same time blocks. These points are replotted in the right panels where panel (f) shows κ_C as a function of $AC(1)$ and panels (g)–(h) show κ_S as a function of $AC(1)$ and as a function of the rate, respectively (r values correspond to linear regression coefficients). The visual stimuli, labeled in panel (a) and denoted by the vertical dashed lines, consisted of a sequence of 8 min. of static gratings (ST) followed by interstimulation period of gray screen, 8 min. of natural images (N), 5 min. of spontaneous activity (Sp), 8 min. of natural images, interstim gray screen, 8 min. of static gratings, interstim gray screen, 5 min. of natural movie (NM), 9 min. of natural images, and 9 min. of static gratings. The symbols in panels (f)–(h) correspond to the different stimuli kinds [colored as the labels on top of panel (a)]. Results computed from Ref. [35].

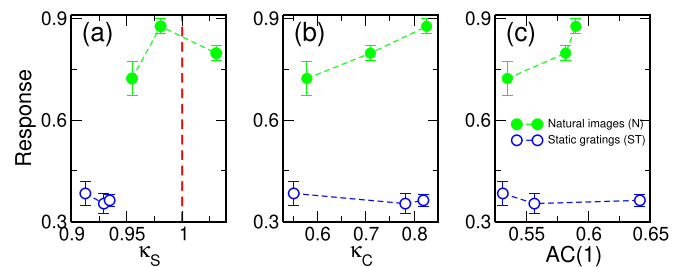


FIG. 8. Changes in the level of response to natural images (N) and static gratings (ST) stimuli as a function of the network state, estimated by the three metrics. Panel (a) corresponds to κ_S , panel (b) to κ_C , and panel (c) to $AC(1)$. For static gratings, the response was computed on the 5 most responsive neurons on each orientation (total: 30 neurons). For natural images, the neurons for the eight natural images with most responsive neurons were considered (natural images 45 with 20 responsive neurons; 85, with 14 neurons; 41, 115, and 108, with 10 neurons; 69 and 36, with 8 neurons; 86 with 7 neurons, total: 87 neurons). All other parameters are the same as in Fig. 7.

advantages, for instance, more immunity to spurious collective effects (noncritical) from a trivial driving by a hidden variable. This cannot be singled out by standard avalanches analysis. In addition, box-scaling should not be affected by subsampling artifacts [7] or overlapping avalanches [9], since the value of $C_W(r)$ is computed from the activity of pairs of *observed* neurons at a distance r .

Regarding the sensitivity of the different observables computed here, we should stress that the definition of κ_S , Eq. (1), computes the signed distance to the expected power-law distribution (instead of, for example, the absolute distance) in such way that positive and negative deviations from the ideal cumulative distribution [as seen in the critical curve of Fig. 1(c), for low and high values of s] compensate. While this makes κ_S robust in the absence of enough data, it also makes it less sensitive. Also, notice that the actual value of κ_S depends on different parameters (such as bin length or threshold c).

$AC(1)$ has a broad peak about the critical point, which makes it an excellent observable for directing the system towards criticality, as discussed already in Ref. [34]. While this feature is shared with the κ_C approach, the latter requires much more information (i.e., to compute from all pairs). Since both peak at the critical point, they cannot be used to distinguish subcritical from supercritical regimes, and some other observable, such as rate or κ_S , has to be used in conjunction to disambiguate. Nevertheless, it should be stressed that supercritical regimes are infrequent in neuronal data.

Notice that, similar to κ_S , $AC(1)$ is computed from the time series of the population activity, which means that it may be subject to external biases and nonstationarities and that they do not profit from spatial information. On the other hand, κ_C can be computed from single time frames, but it cannot be calculated if the neurons' positions are unknown, or in systems where positions are ill defined. Also, as in the numerical results of Ref. [14], we have found in experimental data that the linear relation between r_0 and W at criticality breaks down for very small windows, an observation that deserves further research efforts, and has to be taken into account if κ_C is intended to be used on very-small system sizes.

Overall, numerical simulation results show that the value of the control parameter T_c (i.e., for critical behavior) inferred via avalanche-size distribution is very close to the value that maximizes the correlation length. Thus, the long-term state of

the system can be monitored from either method, although the computation of the correlation length should be more sensitive to dynamic changes, and less dependent on parameters. The analyzed experimental data support this picture.

Many of the results on neuronal activity (including those studied here [35]) on behaving animals are nowadays obtained from optogenetic recordings [16], in which the spike of a neuron (lasting about 1 ms) generates an optical response, related to the displacement of calcium within the neuron, that decays on larger timescales (in the order of a few hundred of milliseconds). Typically, neuronal spikes are inferred through the deconvolution of that signal. However, it has been recently proposed that some analyses, related to different kinds of correlations among pairs of neurons, may be performed without requiring a deconvolution [39]. Although it is not the objective of the present work, the computation of κ_C from minimally preprocessed (i.e., normalized or z scored) calcium data yields results qualitatively similar to those presented above from the inferred spike data. This is a promising avenue for an approach that does not depend on the intricacies of the deconvolution algorithms. The relation between κ_C results obtained from raw calcium signals and from spike data deserves further research, and would likely benefit from the analyses proposed in Ref. [39] (see also Ref. [40]).

In summary, we have explored ways to estimate changes in a network status and introduced a simple metric κ_C describing the typical finite-size behavior of the (instantaneous) spatial correlations of neuronal activity. By construction, κ_C is able to distinguish critical from noncritical dynamics and compares well with avalanche analysis which estimates the distribution of the space-integrated activity. In a given experimental situation, the observation of large κ_C values indicating long-range *spatial* correlations is consistent with the simultaneous observation of large values for the *temporal* correlations, as shown previously [34]. Results presented here suggest that the correlation length computations using box-scaling are well suited as a complement or a substitute of neuronal avalanche analysis as a useful tool for monitoring criticality on diverse experimental conditions.

ACKNOWLEDGMENT

This work was partially supported by Grant No. 1U19NS107464-01 from NIH BRAIN Initiative (USA) and CONICET (Argentina).

-
- [1] P. Bak, *How Nature Works: The Science of Self-Organized Criticality* (Springer Science, New York, 1996).
 - [2] D. R. Chialvo, *Physica A (Amsterdam, Neth.)* **340**, 756 (2004).
 - [3] D. R. Chialvo, *Nat. Phys.* **6**, 744 (2010).
 - [4] J. M. Beggs and D. Plenz, *J. Neurosci.* **23**, 11167 (2003).
 - [5] T. Petermann, T. C. Thiagarajan, M. A. Lebedev, M. A. L. Nicolelis, D. R. Chialvo, and D. Plenz, *Proc. Natl. Acad. Sci. USA* **106**, 15921 (2009).
 - [6] N. Friedman, S. Ito, B. A. W. Brinkman, M. Shimono, R. E. Lee DeVille, K. A. Dahmen, J. M. Beggs, and T. C. Butler, *Phys. Rev. Lett.* **108**, 208102 (2012).
 - [7] T. L. Ribeiro, S. Ribeiro, H. Belchior, F. Caixeta, and M. Copelli, *PLoS One* **9**, e94992 (2014).
 - [8] P. Villegas, S. di Santo, R. Burioni, and M. A. Muñoz, *Phys. Rev. E* **100**, 012133 (2019).
 - [9] D. J. Korchinski, J. G. Orlandi, S.-W. Son, and J. Davidsen, *Phys. Rev. X* **11**, 021059 (2021).
 - [10] J. Touboul and A. Destexhe, *Phys. Rev. E* **95**, 012413 (2017).
 - [11] *Finite-size Scaling*, edited by J. L. Cardy (North Holland, Amsterdam, 1988).
 - [12] D. Fraiman and D. Chialvo, *Front. Physiol.* **3**, 307 (2012).

- [13] A. Haimovici, E. Tagliazucchi, P. Balenzuela, and D. R. Chialvo, *Phys. Rev. Lett.* **110**, 178101 (2013).
- [14] T. L. Ribeiro, S. Yu, D. A. Martin, D. Winkowski, P. Kanold, D. R. Chialvo, and D. Plenz, *bioRxiv* (2020), doi: [10.1101/2020.07.01.182014](https://doi.org/10.1101/2020.07.01.182014).
- [15] S. Camargo, D. A. Martin, E. J. A. Trejo, A. de Florian, M. A. Nowak, S. A. Cannas, T. S. Grigera, and D. R. Chialvo, *arXiv:2206.07797*.
- [16] V. Emiliani, A. E. Cohen, K. Deisseroth and M. Häusser, *J. Neurosci.* **35**, 13917 (2015).
- [17] D. A. Martin, T. L. Ribeiro, S. A. Cannas, T. S. Grigera, D. Plenz, and D. R. Chialvo, *Sci. Rep.* **11**, 15937 (2021).
- [18] M. Zarepour, J. I. Perotti, O. V. Billoni, D. R. Chialvo, and S. A. Cannas, *Phys. Rev. E* **100**, 052138 (2019).
- [19] J. M. Greenberg and S. Hastings, *SIAM J. Appl. Math.* **34**, 515 (1978).
- [20] The computer codes to generate numerical simulation results and data analysis can be found at https://github.com/DanielAlejandroMartin/Kappa_C.
- [21] S. Zapperi, K. B. Lauritsen, and H. E. Stanley, *Phys. Rev. Lett.* **75**, 4071 (1995).
- [22] A. Deluca and A. Corral, *Acta Geophys.* **61**, 1351 (2013).
- [23] W. L. Shew, H. Yang, T. Petermann, R. Roy, and D. Plenz, *J. Neurosci.* **29**, 15595 (2009).
- [24] A. Cavagna, A. Cimorelli, I. Giardina, G. Parisi, R. Santagati, F. Stefanini, and M. Viale, *Proc. Natl. Acad. Sci. USA* **107**, 11865 (2010).
- [25] Q.-Y. Tang, Y.-Y. Zhang, J. Wang, W. Wang, and D. R. Chialvo, *Phys. Rev. Lett.* **118**, 088102 (2017).
- [26] Q.-Y. Tang and K. Kaneko, *PLoS Comput. Biol.* **16**, e1007670 (2020).
- [27] A. Attanasi, A. Cavagna, L. Del Castello, I. Giardina, S. Melillo, L. Parisi, O. Pohl, B. Rossaro, E. Shen, E. Silvestri, and M. Viale, *Phys. Rev. Lett.* **113**, 238102 (2014).
- [28] A. Cavagna, I. Giardina, and T. S. Grigera, *Phys. Rep.* **728**, 1 (2018).
- [29] T. S. Grigera, *J. Phys.: Complex.* **2**, 045016 (2021).
- [30] B. Mariani, G. Nicoletti, M. Bisio, M. Maschietto, S. Vassanelli, and S. Suweis, *Sci. Rep.* **12**, 10770 (2022).
- [31] To compute C_w , in Fig. 3, and related results in Fig. 4, we take information for 1/20 of the 95 000 frames used for computation.
- [32] Alternatively, we propose $r_0(W_i) = a_i(W_i - W_{\min}) + r_0(W_{\min})$ for experimental data, where W_{\min} is the smallest window used.
- [33] Y.-J. Chen, S. Papanikolaou, J. P. Sethna, S. Zapperi, and G. Durin, *Phys. Rev. E* **84**, 061103 (2011).
- [34] D. R. Chialvo, S. A. Cannas, T. S. Grigera, D. A. Martin, and D. Plenz, *Sci. Rep.* **10**, 12145 (2020).
- [35] Allen Institute MindScope Program (2016). Allen Brain Observatory – 2-photon Visual Coding, experimental dataset i.d. 502368172 from container 511510670, available from brain-map.org/explore/circuits. Data recorded (at 30 Hz for 114 099 time frames) from the VISp area of a conscious mice, corresponding to the inferred spike probabilities of 295 neurons inside a field of view of $400 \times 400 \mu\text{m}^2$ and 175 μm depth. Primary publication: S. E. J. de Vries, J. A. Lecoq, M. A. Buice *et al.*, *Nat. Neurosci.* **23**, 138 (2020).
- [36] W. Shew, W. Clawson, J. Pobst, Y. Karimippanah, N. Wright, and R. Wessel, *Nat. Phys.* **11**, 659 (2015).
- [37] Z. Ma, G. Turrigiano, R. Wessel, and K. Hengen, *Neuron* **104**, 655 (2019).
- [38] R. Perin, T. Berger and H. Markram, *Proc. Natl. Acad. Sci. U. S. A.* **108**, 5419 (2011).
- [39] A. Rupasinghe, N. Francis, J. Liu, Z. Bowen, P. O. Kanold, and B. Babadi, *eLife* **10**, e68046 (2021).
- [40] M. Shoutik and B. Babadi, *Adv. Neural Inf. Process. Syst.* **34**, 4120 (2021).